[Research Paper] 대한금속 · 재료학회지 (*Korean J. Met. Mater.*), Vol. 60, No. 4 (2022) pp.321-328
DOI: 10.3365/KJMM.2022.60.4.321

Hydration Deformation Behaviors of Scaffolds of Tricalcium Silicate/Tricalcium Aluminate Mixtures Printed Using the Fused Deposition Modelling (FDM)

Yeongjin Koo[1,2], Myung-Hyun Lee[1], Seog Young Yoon[2], and Yoonjoo Lee[1,*]

[1]*Energy and Environmental Division, Korea Institute of Ceramic Engineering and Technology, Gyeongsangnam-do 52851, Republic of Korea.*
[2]*Department of Materials Science and Engineering, Pusan National University, Busan 46241, Republic of Korea.*

Abstract: 3D printing technology has advanced rapidly over the last decade. However, for ceramic materials, drying and sintering steps are required after printing, and excessive shrinkage that occurs during these steps is a major factor that has hindered the development of the ceramic 3D printing technology. In this study, a non-sintering ceramic 3D printing method was developed using a hydraulic material to overcome the size deformation issue encountered during the post-processing of a scaffold-type printed green body. The deformation characteristics occurring during the curing process were confirmed. Tricalcium silicate (C3S) and tricalcium aluminate (C3A), which are well-known hydraulic materials, were selected. They were prepared into a printable paste by mixing with a viscous hydrophilic oil such as polyethylene glycol and polypropylene glycol, which helped the printout survive without collapse while it was cured. The scaffold was printed by Fused Deposition Modelling (FDM), which is the simplest and most economical printing method, and was cured by immersion in a water bath. The hydrated scaffold of the C3S/C3A mixture exhibited a smaller strain than the scaffold of the single materials, and the deformation amount depended on the printing direction. Remarkably, a scaffold with the smallest deformation, of less than 1%, and the highest compressive strength was obtained with a C3S/C3A mixing ratio of 65/35.

(Received November 29 2021; Accepted December 20, 2021)

Keywords: 3D printing, additive manufacturing, sintering-free, cement scaffold, FDM process, size deformation

1. Introduction

A key advantage of 3D printing technology is that it can be used as a small quantity batch production system. 3D printing technologies for plastic and metallic materials have been developed rapidly over the past decade and also applied in industries. Currently, there is great demand for a 3D printing technique that allows precise shape control and customizable design in the medical field. 3D printing technologies using ceramics are being developed with suitable dental and surgical materials such as alumina, zirconia, and calcium phosphate. The manufacturing of artificial porous bodies has been attempted for a long time for biomedical processes such as orthopedic surgeries or tissue engineering which require a porous ceramic support as a scaffold, [1-3]; however, there have been only a few commercially successful examples so far. Moreover, compared to existing processes, 3D printing techniques can not only provide a durable porous material, but allow control over the shape and porosity of the scaffold [4-6].

In ceramic 3D printing, it is necessary to control the various processes that occur during printing and post-processing, in addition to the characteristics of the printing material. The most common and important factors when producing ceramic materials is that they require drying, debinding, and heat-treatment steps after printing, regardless of the printing method, because shrinkage and deformation occur in each step and cannot be prevented [7-9]. This issue of shape deformation is encountered even when materials that do not require sintering are used. For example, certain ionic materials that may be cured using water undergo deformation during the curing process.

Calcium compounds are typical hydraulic materials and

- 구영진: 학생연구원, 이명현: 수석연구원, 윤석영: 교수, 이윤주: 책임기술원
**Corresponding Author:* Yoonjoo Lee
[Tel: +82-55-792-2611, E-mail: yoonjoo_lee@kicet.re.kr]

have been studied for a long time in the field of bioceramics, as well as being investigated as 3D printing materials [10-12]. To guarantee numerical stability and durability, it is necessary to determine the states that occur during printing or post-processing, and then to resolve those issues during the curing process. The hydration of calcium-based materials involves different reaction mechanisms or reaction kinetics depending on the material type, and it is common to use a mixture of materials rather than a single one to produce ceramic products [13,14]. Calcium silicate compounds are materials whose strength increases over time, and amongst them, C3S is known to have the highest strength. However, because it has a slow hydration reaction, C3A, which has a fast reaction rate, is typically added to compensate [15].

Tricalcium silicate (C3S) and tricalcium aluminate (C3A) are the well-known main components of Portland cement, and as representative hydraulic materials have also been used as dental fillers and bone cement materials for a long time. While previous studies have mainly focused on the structural characteristics of the scaffold or the bioactivity of the materials [16-18], in this study, the deformation characteristics of the C3S/C3A mixture were investigated to develop a sintering-free ceramic 3D printing technology. An FDM (fused deposition modeling) printer, which is the most economical, fastest, and simplest printer, was used for printing, and the compressive strength of the hydrated scaffold was evaluated.

2. Experimental

2.1 Materials

$CaCO_3$ (99.9%, Kojundo Chemical Co. Ltd., Japan), SiO_2 (99.9%, Kojundo Chemical Co. Ltd., Japan), and Al_2O_3 (99.7%, Junsei Chemical Co. Ltd., Japan) were used as starting materials to prepare the C3S ($3CaO{\cdot}SiO_2$) and C3A ($3CaO{\cdot}Al_2O_3$). SiO_2 or Al_2O_3 was mixed with $CaCO_3$ at a ratio of 1:3 with water, molded into a sphere, and then heated at 1600 or 1400 °C, respectively. The synthesized C3S and C3A spheres were then ground and sieved through a 325 mesh screen.

2.2 Printing of scaffolds

To prepare the printing paste, polypropylene glycol (PPG; P400, Sigma-Aldrich, USA) and polyethylene glycol (PEG, tested according to Ph. Eur., 1,000, Sigma-Aldrich, USA) were used as the media or binders. The total content of the C3S and C3A mixed powder was 40–50% of the paste. The mixing ratios of the C3A and C3S are listed in Table 1.

Table 1. Mixing ratios of C3A and C3S

Sample name	Mixing ratio (wt.%)	
	C3S	C3A
C3S	100	-
C3S80	80	20
C3S70	70	30
C3S65	65	35
C3S50	50	50
C3A	-	100

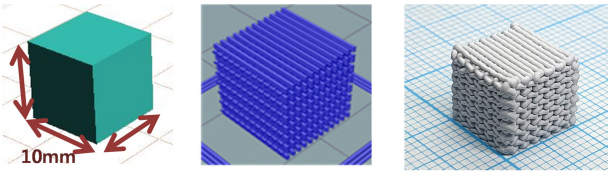

(a) (b) (c)

Fig. 1. (a) A 10×10×10 mm cube model, (b) scaffold shape modeling, and (c) hydrate printout.

The viscosity of the printing paste was measured at 5×10^3 – 10 Pa·s to be in the range of shear rate 0.1 – 100 /s using the parallel plate method of a rotational viscometer. The ceramic paste was filled into a cylinder equipped with a 400 μm diameter nozzle and was printed using an INVIVO premium printer (Rokit Healthcare, Republic of Korea) under the following conditions: an extrusion amount of 2.0%, interlayer thickness of 320 μm, molding speed of 25 mm/s, and at room temperature. A scaffold was modeled by applying a 50% infill mode to a space of 10×10×10 mm using Creator K (a file conversion program supplied by Rokit Healthcare). By setting the wall thickness to zero, the extruded filaments were arranged at regular intervals and cross-stacked at a 90° angle for every layer (see Fig. 1(a) and (b)). The printed green body was immersed in distilled water for 18 hours to be hydrated without a drying step, and then the scaffold was dried at 60 °C after rinsing with distilled water. A cured scaffold was obtained, as shown in Fig. 1(c).

2.3 Analysis

Isothermal calorimetry was performed to evaluate the heat of hydration of the ceramic material using a three-point multipurpose conduction calorimeter (Tokyo-Riko Co. Ltd., Japan). For this analysis, the as-prepared ceramic paste employed for printing was used. The compressive strength of the scaffold was measured at a cross-head speed of 0.5 mm/min using an Amsler universal tester (RB301, R&B, Republic of Korea), and the porosity of the scaffold was determined under 30,000 psi using a mercury porosimeter. (Autopore IV 9500, Micromeritics, USA)

3. Results and Discussion

3.1 Hydration of calcium compounds

In the preparation of a printable paste, the filling quantity and dispersion of the powder are generally considered first, to improve the packing density of the particles. To design a paste suitable for FDM printing, it is necessary to select the appropriate media and additives, ones that will allow control over the rheological behavior of the printing paste, considering the extrusion effect and drying that occurs during the printing process [19,20]. C3S and C3A, which are hydraulic materials, need a curing process after the printing step. They therefore require a water supply system for the hydration reaction and an appropriate system for maintaining the state of the printed product during the hydration reaction. For example, Yoon used a double nozzle to simultaneously extrude water and paste to induce a curing reaction during the printing process, while Kim and Lee induced the curing of the printed material by placing the nozzle in a water bath and printing in water [21,22].

In the present study, a two-step process was applied, treating the printing and hardening steps separately. A commercial printer was used without any particular modification of the equipment. First, printing was performed using the ceramic paste, and then the printed product was immersed in water for hardening. However, an important issue needs to be considered in this case: when the printed product is immersed in water, the printed material and water molecules diffuse in opposite directions, resulting in swelling, and the product shape cannot be maintained (see Fig. 2(a)). Therefore, the printing paste needs to be formulated to ensure that the printed green body survives as it hardens upon immersion in water.

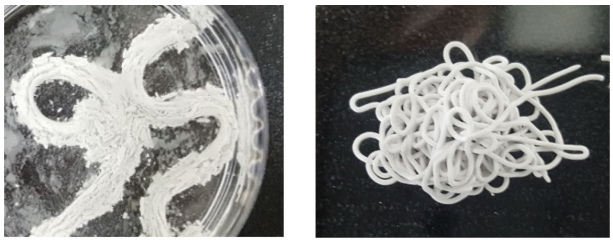

(a) (b)

Fig. 2. Photographs of (a) an inflated filament and (b) a filament that maintained its state when cured in a water bath. A C3S/C3A mixture was used for printing.

In this study, a viscous oil was used instead of an alcohol or organic solvent to prevent shrinkage issues during the drying process. PEG and PPG, which are water-miscible hydrophilic oils, were selected as dispersion media. After the C3S/C3A powder mixture was blended with the oil, the paste was injected using a 400 μm nozzle and then immersed in a water bath. As shown in Fig. 2(b), the injected material cured without any collapse or swelling, confirming that PEG and PPG are appropriate media for preparing the printing paste with the water-curable materials used in this study.

As C3S and C3A undergo hydration, the reaction time and calorific value are different for each material. To ensure a sufficient curing time, the reaction kinetics of each material were studied. The heat of hydration was measured using the as-prepared mixture. According to the exothermic curve (Fig. 3(a)), the reaction of C3S began slowly and proceeded for ~18 h, showing the highest reaction rate at 10 h. The hydration mechanism of C3S is as follows: one half of the calcium combines with water molecules, while the other half is converted to $Ca(OH)_2$ crystals (Eq. 1). On the other hand, C3A absorbs twice of water molecules as C3S (Eq. 2), but does not form new crystals and has a very fast reaction rate (Fig. 3(a)).

$$\text{C3S: } 2(3CaO{\cdot}SiO_2) + 6H_2O \rightarrow 3CaO{\cdot}2SiO{\cdot}3H_2O + 3Ca(OH)_2 \quad (1)$$

$$\text{C3A: } 3CaO{\cdot}Al_2O_3 + 6H_2O \rightarrow 3CaO{\cdot}Al_2O_3{\cdot}6H_2O \quad (2)$$

The isothermal calorimetry curves showing the hydration heat of different C3S/C3A mixtures are presented in Figure 3(b). The results suggest a change in the heat of hydration

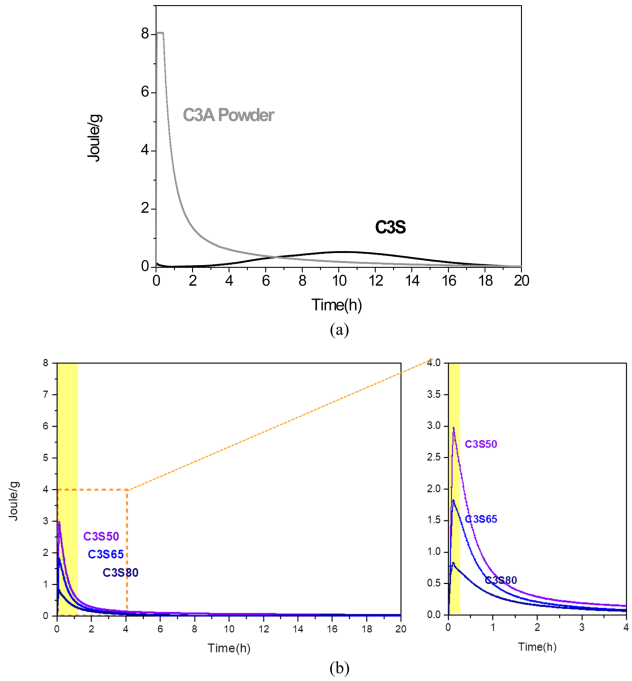

Fig. 3. Hydration heat curves of the printable pastes of (a) single materials and (b) mixtures of C3S and C3A.

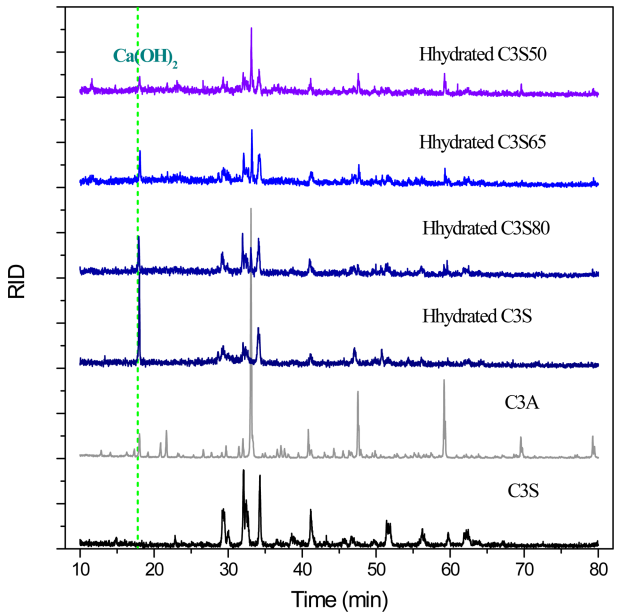

Fig. 4. X-ray diffraction patterns of C3S, C3A, and the hydrates of C3S/C3A mixtures

curve depending on the mixing ratio of the two components. It was not clear whether both materials influenced the total reaction rate. Therefore, in this study, the printed product was immersed in water for 18 h for curing, according to the

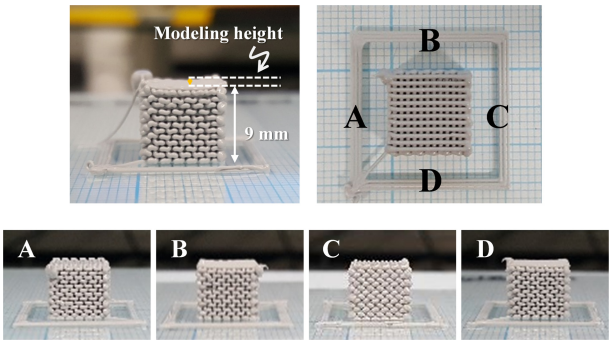

Fig. 5. Printed scaffold from different viewing angles.

curing time of C3S.

The completion of the reaction was confirmed by X-ray diffraction analysis. For the C3S, the intensities of the main peaks at 32° and 34° decreased noticeably after hydration, and a new peak appeared at 18° (Fig. 4). Meanwhile, C3A did not show a significant change in its phase before and after the hydration reaction; only the intensity of the main peak at 33° changed according to the mixing ratio.

3.2 Printing characteristics and hydration of the single materials

Fig. 1 compares the modeling image and the form of the scaffold printed using the FDM printer. In the printing step, the nozzle moved along the designed path in accordance with the model size of 10×10×10 mm, and the paste was extruded in the form of filaments and stacked with a uniform thickness and spacing (Fig. 5). The viscosity of the printed paste remained the same as that before printing, making it difficult to measure the actual size. Therefore, its size was determined based on the printing path and the thickness of the filament ejected from the nozzle. The print path was adjusted to the contour of the model size, and the diameter of the printed filament was ~500 μm (Fig. 6); based on this, the size of the product along the *xy*-plane was estimated to be approximately 10.5×10.5 mm (*x*×*y*). As the number of printing layers increases, the printed product composed of the viscous paste may deform under the weight of the stacked material. The height of the printed product was measured to be 9 mm, which is shorter than the intended size of 10 mm. This is because the printed form of viscous paste likely deformed as the number of printing layers increased (Fig. 5).

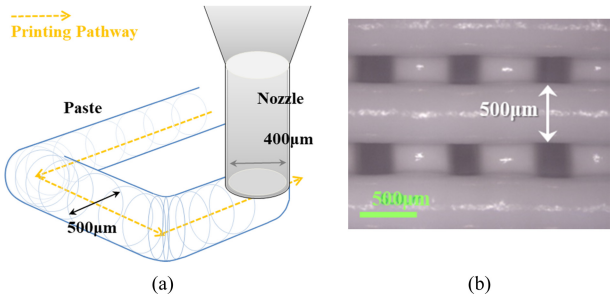

Fig. 6. (a) Printing pathway with the filament width and (b) the measured filament diameter after printing.

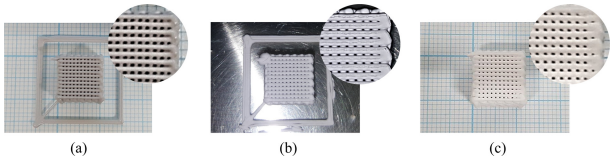

Fig. 7. Shapes of (a) an as-printed scaffold and (b, c) hydrated scaffolds of (b) C3S and (c) C3S.

Therefore, the changes in size and compressive strength were measured after hardening a scaffold of 10.5×10.5×9 mm.

Fig. 7(b) and (c) show the hydrated scaffolds of C3S and C3A, respectively. Comparing the size and shape of the hydrates with those of the printed material immediately after printing (Fig. 7(a)) revealed that the overall filament size increased and the thickness of the filament constituting the internal skeleton increased during the hydration process. It is noteworthy that cracks appeared on the surface of the filaments formed in the printing direction in the scaffold made of C3S, which had a slow reaction rate. As shown in the example in Fig. 2, it is important to control the diffusion of water molecules and paste components occurring in water to maintain the shape of the printed product. Although the scaffold formed with C3A expanded, it maintained its shape without defects because C3A can quickly hydrate, and this prevents the paste from diffusing into the water. In contrast, when the C3S paste is immersed in water it might expand as water diffuses into it during the curing reaction. As a result, the internal parts of the paste swelled and cracked while the shape of the filament surface was maintained.

3.3 Hydration deformation behavior of the C3S and C3A mixture

Fig. 8(a) shows the completely cured scaffolds of C3S/C3A mixtures with different C3S/C3A ratios of 70/30, 65/35, and 50/50. Based on visual observation, the samples did not exhibit any significant deformation. The filaments were regularly arranged and the pore distribution was uniform. It is worth noting that the change in size of these scaffolds depends on the C3S/C3A mixing ratio. Moreover, the deformation depends on the direction of printing since the expansion rate in the *xy*-plane (*x*- and *y*- axes) was larger than that along the *z*-axis (Fig. 9). The C3S65 scaffold, prepared using a mixture with a C3S/C3A ratio of 65/35, had a size of 10.6×10.6 mm in the *xy*-plane with an expansion rate of less than 1%; that is, the smallest size change. Considering that the cross-sectional diameter of the filament was 570 μm in this condition (Fig. 10), the size of the scaffolding expansion and the change in filament diameter were approximately the same. This indicates that the total change in size of this scaffold was due to the expansion of the filament skeleton. As the content of C3S or C3A was changed from the mixing ratio of C3S65, the overall size of the hydrate increased, but the change in the size in the specimens was not large compared to that of C3A (Fig. 8(b)).

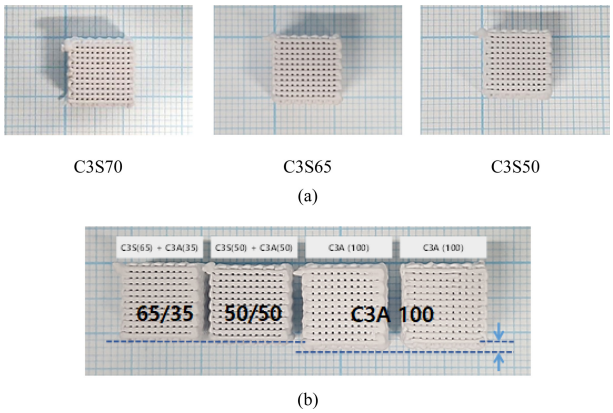

Fig. 8. (a) Hydrated scaffolds of C3S/C3A mixtures and (b) comparison of the size differences.

As mentioned above, the scaffold hardening results from a chemical reaction. Since the reaction is induced by water, the water diffusion rate might be an important factor that affects the shape maintenance. The results of a simple diffusion test showed that viscous hydrophilic oil helped to maintain the printout shape and prevent collapse (Fig. 2), but the oil cannot selectively control the diffusion rate of water molecules, which is based on the mixing ratio of C3S and

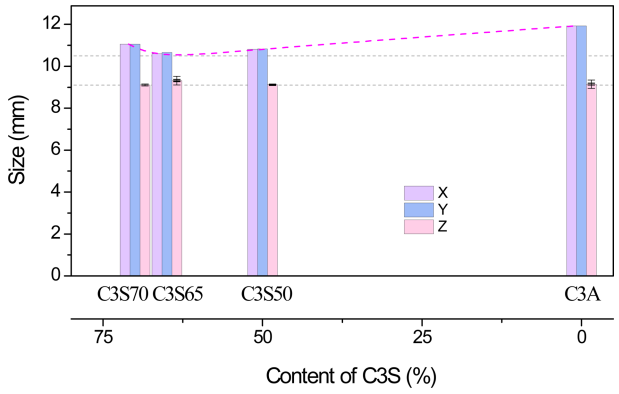

Fig. 9. Expanding behavior of the scaffolds at different mixing ratios of C3S and C3A.

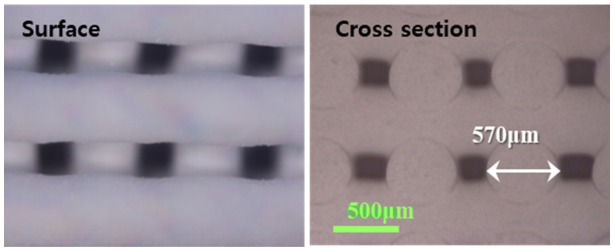

Fig. 10. Surface and cross-sectional images of a hydrated C3S/C3A scaffold.

C3A. Therefore, because the hydration reaction rates of C3S and C3A were complementary, the printed mixture could be more stably cured compared to a single printed material. The expansion behavior appeared to differ depending on the mixing ratio of the two components.

As shown in Fig. 9, the deformation of the scaffold differed depending on the direction: the expansion along the *z*-axis was smaller than that along the *xy*-plane. This is because the shape is also a factor that determines the size change when the hydration reaction occurs. For example, for a small spherical model, deformation occurs evenly along the *x*-, *y*-, and *z*-axes ($\Delta x = \Delta y = \Delta z$; Fig. 11(a)). However, in a unidirectional model such as a filament, expansion in the *y*- and *z*-directions with empty spaces between filaments is better compared to expansion in the *x*-axis, corresponding to the longitudinal direction ($\Delta x < \Delta y, \Delta z$; Fig. 11(b)). Even in the case of a laminated filament structure, the size deformation will proceed in the direction the nozzle moved, leading to an increase in volume in the *xy*-plane especially, and therefore, the expansion in the lamination direction will be suppressed ($\Delta b < \Delta a$, Fig. 11(c)). Even with a structure of laminated filament, the filament expands into the void space (Δb, $\Delta c < \Delta a$, Δd Fig. 11(c)), and consequently, the expansion in the stacking direction is suppressed ($\Delta z < \Delta x$, Δy; Fig. 11(d)). Therefore, C3A did not show any significant change in height despite the 13% change in the *xy*-plane of the scaffold following hydration.

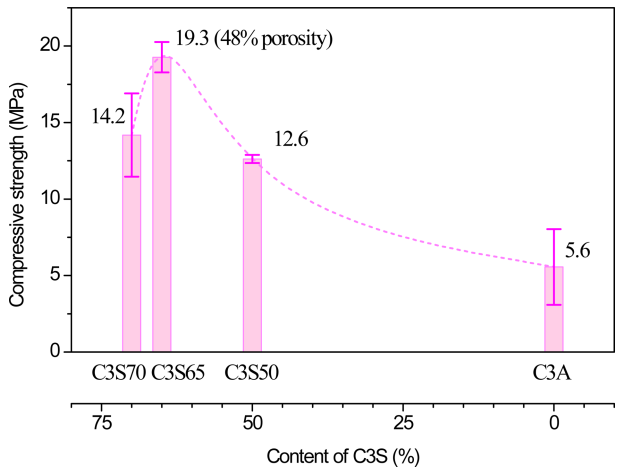

Fig. 12. Compressive strengths of C3S/C3A scaffolds with different mixing ratios of C3S and C3A.

Figure 12 shows the compressive strengths of the scaffolds. The scaffold of C3S65 had the highest strength, and the strength showed a tendency to decrease as the amount of C3S or C3A was increased with respect to that of C3S65. Because hydration-induced deformation causes expansion of the filaments constituting the scaffold, as well as the size of the

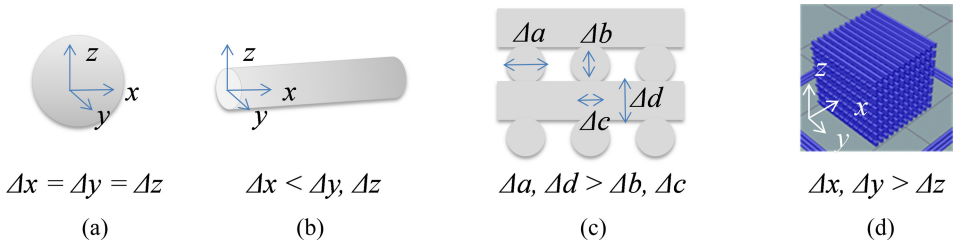

Fig. 11. Expansion direction of hydrating materials of various shapes.

specimen itself, the porosity of the scaffold changes according to the mixing ratio. For example, the porosity of the C3S65 scaffold was approximately 48%, whereas the porosities of the scaffolds with other compositions were lower, owing to higher filament expansion. Nevertheless, the C3S65 scaffold exhibited the highest strength because the intrinsic properties of the material are the main factors that determine the mechanical properties, even in the case of porous materials.

In addition, in this study, because the compressive strength behavior of the scaffold according to the mixing ratio followed the deformation behavior, it can be stated that the deformation properties were more dominant than the structural characteristics. Therefore, even in the case of a water-curable material, deformation due to the diffusion or contraction of the material is an important factor and influences the mechanical properties of the resulting printed structure.

4. Conclusion

In this study, a porous scaffold with a lattice structure was printed using the hydraulic materials C3S and C3A, and its deformation behavior was investigated to develop a non-sintered ceramic 3D printing method. To prevent the drying-induced deformation, PEG and PPG were used as the media or binders without a solvent, and the hydration reaction of the printed material was induced by the diffusion of water into the printed material. The green bodies printed with the single materials of C3S and C3A expanded noticeably, regardless of the hydration rate of each material. However, the printed materials composed of the C3S/C3A mixture cured more stably, probably because the two types of materials with different hydration rates could suppress the diffusion rates of the paste and water molecules during the curing process.

The deformation behavior of the mixture depended not only on the C3S/C3A mixing ratio, but also on the printing or stacking direction. Scaffolds stacked in a lattice shape have empty spaces, which aid the local expansion of the filament. In the case of C3S65, the thickness of the filament increased, but the total size of the scaffold changed by <1%. On the other hand, as the amount of C3S or C3A increased with respect to that of the C3S65 mixture, expansion of the scaffold was observed, and the expansion occurred mainly along the *xy*-plane, but not along the *z*-axis. In addition, the expansion behavior, which changed with the C3S/C3A mixing ratio, influenced the mechanical properties of the scaffold. The C3S65 scaffold with a C3S/C3A mixing ratio of 65/35, which had the smallest hydration strain, exhibited the highest compressive strength, although it had the highest porosity.

Acknowledgement

This research was financially supported by the Institute of Civil Military Technology Cooperation funded by the Defense Acquisition Program Administration and Ministry of Trade, Industry and Energy of Korean government under grant No.21-CM-CE-03. And it was supported by the Korea Institute Ceramic & Engineering under grant No.KCS19010-1.

REFERENCE

1. M. E. Norman, H. M. Elgendy, E. C. Shors, S. F. El-Amin, and C. T. Laurencin, *Clin. Mater.* **17**, 85 (1994).
2. I. K. Jun, Y. H. Koh, and H. E. Kim, *J. Am. Ceram. Soc.* **89**, 391 (2006).
3. Y. Wen, S. Xun, M. Haoye, S. Baichuan, C. Peng, L. Xuejian, Z. Kaihong, Y. Xuan, P. Jiang, and L. Shibi, *Biomater. Sci.* **5**, 1690 (2017).
4. A. Koyyada and P. Orsu, *Regen. Eng. Transl. Med.* 7, 147 (2021).
5. J. Roleček, L. Pejchalová, F. J Martínez-Vázquez, P. Miranda González, and D. Salamon, *J. Eur. Ceram. Soc.* **39**, 1595 (2019).
6. U. Deisinger, S. Hamisch, M. Schumacher, F. Uhl, R. Detsch, and G. Ziegler, *Key. Eng. Mater.* **361**, 915 (2008).
7. F. Pourcel, W. Jomaa, J. R Puiggali, and L. Rouleau, *Drying Technol.* **25**, 759 (2007).
8. A. R Boccaccini and P. A Trusty, *Mater. Charact.* **41**, 109 (1998).
9. Z. Fu, P. Polfer, T. Kraft, and A. Roosen, *J. Eur. Ceram. Soc.* **35**, 2413 (2015).
10. C. Yang, X. Wang, B. Ma, H. Zhu, Z. Huan, N. Ma, C. Wu, and J. Chang, *ACS Appl. Mater. Interfaces.* **9**, 5757 (2017).
11. Y. H Lin, Y. C Chiu, Y. F Shen, Y. H. A Wu, and M. Y Shie, *J. Mater. Sci. Mater. Med.* **29**, 11 (2018).
12. G. Zhao, R. Cui, Y. Chen, Si. Zhou, C. Wang, Z. Hu, X.

Zheng, M. Li, and S. Qu, *J. Bionic. Eng.* **17**, 652 (2020).
13. W. N. Liu, J. Chang, Y. Q. Zhu, and M. Zhang, *Int. Endod. J.* **44**, 41 (2011).
14. M. A. Saghiri, J. Orangi, A. Asatourian, J. L. Gutmann, F. G. Godoy, M. Lotfi, and N. Sheibani, *Dent. Mater. J.* **36**, 8 (2017).
15. Q. S. Bach, *Applied Mechanics and Materials* **889**, 294 (2019)
16. J. S. Lee, H. D. Cha, J. H. Shim, J. W. Jung, J. Y. Kim, and D.W. Cho, *J. Biomed. Mater. Res.* **100A**, 1846 (2012).
17. S. Amirkhani, R. Bagheri, and A. Z. Yazdi, *Acta. Materialia.* **60**, 2778 (2012).
18. S. C. Kapfer, S. T. Hyde, K. Mecke, C. H. Arns, and G. E. Schröder-Turk, *Biomaterials.* **32**, 6875 (2011).
19. R. O'Neill, H. O. McCarthy, E. Montufar, M-. P. Ginebra, D. I. Wilson, A. Lennon, and N. Dunne, *Acta. Biomater.* **50**, 1 (2017).
20. H. Liu and M. C. Leu, *Int. J. Mod. Phys. B.* **23**, 1861 (2009)
21. H. S. Yoon, *Methods for preparing bone cement scaffold and bone cement scaffold prepared thereby*, http://m.kipris.or.kr/mobile/search/view_patent.do?applno=1020110091929 (2011).
22. H. W. Kim and G. S. Lee, *A preparation method of porous scaffolds of calcium phosphate cement*, KR10-1686683.